CHEMISTRY OF MATERIALS

Article

pubs.acs.org/cm

Amorphous TiO_2 Buffer Layer Boosts Efficiency of Quantum Dot Sensitized Solar Cells to over 9%

Zhenwei Ren,[†,⊥] Jin Wang,[†,⊥] Zhenxiao Pan,[†] Ke Zhao,[†] Hua Zhang,[†] Yan Li,[†] Yixin Zhao,[‡] Ivan Mora-Sero,[§] Juan Bisquert,[§,∥] and Xinhua Zhong*[,†]

[†]Key Laboratory for Advanced Materials, Institute of Applied Chemistry, East China University of Science and Technology, Shanghai 200237, China

[‡]School of Environmental Science and Engineering, Shanghai Jiao Tong University, Shanghai 200240, China

[§]Institute of Advanced Materials (INAM), Universitat Jaume I, 12006 Castelló, Spain

[∥]Department of Chemistry, Faculty of Science, King Abdulaziz University, Jeddah, Saudi Arabia

Supporting Information

ABSTRACT: Charge recombination at an electrode/electrolyte interface is the main factor to limit the power conversion efficiency (PCE) of quantum dot sensitized solar cells (QDSCs). Herein, we present a novel and facile strategy based on successive coating of a sensitized electrode with a combination of blocking layers in appropriate sequence for suppressing the charge recombination. In this scenario, modification of the exposed surface of both TiO_2 particles and QDs with an amorphous TiO_2 (am-TiO_2) layer via a classical $TiCl_4$ hydrolysis treatment plays a fundamental role to enhance the effectiveness of a recombination blocking ZnS/SiO_2 barrier layer. This strategy allows construction of $CdSe_{0.65}Te_{0.35}$ QD based champion QDSCs exhibiting a new PCE record of 9.28% and a certified PCE of 9.01% under full one sun illumination. The specific nature and sequence of the layering process is critical for the gain of photovoltaic performance. Control experiments indicate that the am-TiO_2 is superior to a crystalline TiO_2 layer in serving as the passivation/buffer layer and improving the photovoltaic performance of the cells. Insight from impedance spectroscopy (IS) and open circuit voltage decay (OCVD) measurements demonstrates that when the am-TiO_2 layer is located at the interface between the QD sensitized photoanode and the ZnS/SiO_2 barrier layer, it inhibits remarkably the charge recombination at the photoanode/electrolyte interface and prolongs the electron lifetime.

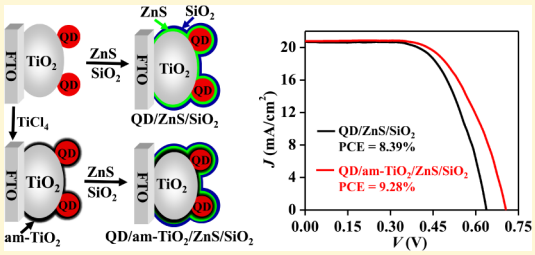

INTRODUCTION

Exploiting solar energy is believed to be of great potential to solve social concerns such as the exhaustion of fossil fuels, as well as global warming. The most direct way to harvest the solar energy is to convert sunlight into electricity using photovoltaic technology.[1−3] Being a promising low-cost candidate for third generation photovoltaic cells, quantum dot sensitized solar cells (QDSCs) are attracting increasing academic and industrial interest due to the unique properties of QD light-absorbers, such as solution processability, band gap tunability, high absorption coefficient, and multiple exciton generation possibility.[4−8] However, charge recombination at TiO_2/sensitizer/electrolyte interfaces is more severe for QDSCs than for their analogous dye sensitized solar cells (DSCs),[9−12] limiting the efficiency of the former type of cells. This fact is due to the existence of surface trap states in QDs and to the large fraction of uncovered surface of the TiO_2 electron conductor, which act as recombination centers for photoinjected electrons in the TiO_2 with holes in sensitizers or oxidized species in redox electrolyte. Charge recombination leads to the loss of charge carriers and therefore decreases the photovoltaic performance of the cell devices, affecting especially the photovoltage of the device.[9−14] This is one of the main reasons that limits the power conversion efficiency (PCE) of QDSCs, with the best ones at the level of 6−8%.[12,15−22] In order to attain these results, coating of the sensitized electrode has to be performed. Very recently, charge recombination occurring at the photoanode/electrolyte interface in QDSCs has been significantly and effectively reduced via wide band and insulator ZnS/SiO_2 barrier layer overcoating around the QD sensitized photoanode. The resulting TiO_2/QD/ZnS/SiO_2 configuration based CdSeTe QDSCs exhibited the highest reported certified efficiency for QDSCs of 8.2%.[19] In that work, the external quantum efficiency (EQE) has been improved to a near theoretical up-limit of about 80%. However, there is a huge gap between the obtained open-circuit voltage (V_{oc}, 0.64 V) and the optical band gap (~1.5 eV) of the CdSeTe QD light-absorber. This demonstrates that, on one hand, there is an enormous space for the further improvement of PCE in this kind of QDSC;[23] on the other hand, the photovoltage

Received: October 1, 2015
Revised: November 24, 2015

DOI: 10.1021/acs.chemmater.5b03864
Chem. Mater. XXXX, XXX, XXX−XXX

enhancement would be imperative for the further improvement of PCE. For the improvement of photovoltage, one of the most straightforward strategies is to passivate the photoanode surface state in order to reduce recombination. Undoubtedly, the big lattice mismatch between TiO_2 substrate and ZnS interface (7%) as well as CdSeTe and ZnS interface (14%) in the above-reported QDSC system would induce an incomplete photoanode passivation,[24,25] and further blocking effect should be expected with an appropriated strategy.

Overcoating a barrier layer of insulating or wide band gap materials around a TiO_2 surface has been a widely accepted concept for the reduction of charge recombination in both DSCs[26−33] and QDSCs.[19,34−39] In previously reported DSCs, limited by the physicochemical stability of molecular dyes, the target barrier layers are usually overcoated on a plain TiO_2 film electrode prior to its sensitization by dye molecules.[26−33] The classical approach for this barrier layer deposition is the $TiCl_4$ solution treatment, wherein an extra crystalline TiO_2 layer, derived from $TiCl_4$ hydrolysis followed by sintering at high temperature (typically at 400−500 °C) is overcoated around the TiO_2 nanoparticles constituting the film.[30−33] It has been demonstrated that this treatment can significantly improve the photocurrent of the resulting DSC cells due to the suppression of charge recombination owing to the decreased surface traps of TiO_2 electron conductor and the increased loading of dye molecule sensitizers.[30−33] Unfortunately, previous reports show that this $TiCl_4$ treatment with formation of a crystalline TiO_2 layer on a plain TiO_2 electrode has a negligible effect on the improvement of photovoltaic performance in QDSCs,[40,41] but a positive effect was also reported based on CdS QDSCs with poor performance.[42,43]

Herein, we report for the first time the application of an amorphous TiO_2 (abbreviated as am-TiO_2 henceforth) passivation/buffer layer between the QD sensitized photoanode and ZnS/SiO_2 barrier layer interfaces to decrease the trap state defects induced by the large lattice mismatch between the interfaces and therefore suppress the charge recombination and enhance photovoltaic performance. This novel am-TiO_2 passivation layer is prepared in a facile way by a $TiCl_4$ aqueous solution hydrolysis process at low temperature after the deposition of QDs on a TiO_2 film electrode and avoiding any further high temperature sintering treatment. It is demonstrated that this am-TiO_2 passivation layer located between the sensitized photoanode and ZnS/SiO_2 barrier layer interfaces has a rather large effect on improving the performance, especially the photovoltage of the resulting QDSCs compared to this am-TiO_2 passivation layer located on different positions (i.e. between ZnS and SiO_2 coating layers, or outside the ZnS/SiO_2 layer). It is noted that coating of sensitized QD photoanodes with a sole am-TiO_2 layer has been previously developed.[35,44,45] However, both our own experimental results and literature results demonstrate that a sole am-TiO_2 layer overcoating cannot offer dramatic improvement of PCE of the resulting cell devices, highlighting the synergistic effect between am-TiO_2 and ZnS/SiO_2 barrier layers proposed here. Impedance spectroscopy (IS) and open circuit voltage decay (OCVD) measurements show that this am-TiO_2 passivation layer significantly reduces the electron recombination at the photoanode/electrolyte interfaces while other energetic features of the photoelectrode such as the position of the conduction band edge remain unchanged. As a consequence, the electron lifetime was prolonged by several times. The constructed CdSeTe QD based QDSCs exhibit an unprecedented PCE of 9.28% and a certified efficiency of 9.01% under AM 1.5G full one sun illumination. The obtained high efficiency QDSCs via am-TiO_2 passivation interface engineering suggest a promising strategy to further push QDSCs to a higher efficiency level.

EXPERIMENTAL SECTION

Chemicals. Selenium powder (99.99%), cadmium oxide (CdO, 99.99%), tellurium powder (200 mesh, 99.8%), 1-octadecene (ODE, 90%), trioctylphosphine (TOP, 90%), oleyl amine (OAm, 95%), and sulfur (S, 99%) were purchased from Aldrich. Oleic acid (90%) and thioglycolic acid (TGA, 97%) were obtained from Alfa. Paraffin liquid (chemical grade), tetraethyl orthosilicate, titanium tetrachloride ($TiCl_4$, 99%), sodium sulfide (Na_2S, 98%), zinc acetate ($Zn(OAc)_2$, 99%), and all solvents (analytical grade) were obtained from Shanghai Chemical Reagents Company (China).

QD Synthesis and TiO_2 Film Electrode Preparation. The synthesis of CdSeTe or CdSe QDs, ligand exchange for obtaining thioglycolic acid (TGA)-capped water-soluble QDs, and the deposition of these water-soluble QDs on TiO_2 film electrodes are all referred to our previous work.[19,22] Double layer TiO_2 mesoporous film electrodes were prepared by a screen printing method on a cleaned F:SnO_2-coated conducting glass (FTO, 8 Ω/square) according to a literature method.[41] Normally, a 9.0-μm-thick transparent layer of 20−40 nm sized TiO_2 particles (P25, Degussa) was first prepared on the FTO glass and then covered with a 6.0-μm-thick light scattering layer of 400 nm sized TiO_2 particles. Finally, the film was sintered in a muffle at 500 °C for 30 min.

Photoanode Treatment. The $TiCl_4$ treatment was employed on both a plain TiO_2 film electrode and QD sensitized TiO_2 film electrodes. For the treatment on the plain electrode, the as-prepared TiO_2 film electrodes were immersed in the $TiCl_4$ aqueous solution (containing 0.01 M $TiCl_4$ and 0.01 M TGA) for 30 min at 40 °C followed by rinsing with water and ethanol sequentially. After that, the films were immersed in QDs solution for QD deposition. As for the treatment on the sensitized electrode, the QDs sensitizer was first deposited onto the TiO_2 films, and then the sensitized electrodes were immersed in the $TiCl_4$ solution as mentioned above. Eventually, all the electrodes that had undergone different $TiCl_4$ treatment processes were coated with four cycles of ZnS by immersion into 0.1 M $Zn(OAc)_2$ and 0.1 M Na_2S solutions in aqueous solutions for 1 min/dip alternately and then coating with a SiO_2 layer by soaking the electrodes in 0.01 M tetraethyl orthosilicate ethanol solution for 2 h followed by rinsing with ethanol and drying in air.

Assembling Solar Cells. The sandwich-type cells were constructed by assembling the photoanode and the $Cu_{2-x}S$/FTO counter electrode using a 50-μm-thick Scotch spacer, and they were filled with a 10-μL polysulfide electrolyte. The $Cu_{2-x}S$/FTO counter electrode were prepared according to the literature method.[46] The polysulfide electrolyte aqueous solution consists of 2.0 M Na_2S, 2.0 M S. For QDSCs studied under each condition, five cells were prepared in parallel, and the average values were used to evaluate their performance.

Characterization. Photovoltaic performances ($J-V$ curves) of cell devices were recorded on a Keithley 2400 source meter under illumination by an AM 1.5 G solar simulator (Oriel, model no. 91160, equipped with a 150W xenon lamp). The power of the simulated light was calibrated to 100 mW/cm^2 by an NREL standard Si solar cell. The photoactive area was 0.1276 cm^2, defined by a metallic black mask. The EQE was recorded on a Keithley 2000 multimeter under the illumination of a 300 W tungsten lamp with a Spectral Products DK240 monochromator. Impedance spectroscopy measurements (IS) were carried out on an impedance analyzer (Zahner, Zennium) under dark conditions at forward bias ranging from 0 V to higher than V_{oc}, applying a 20 mV AC sinusoidal signal over the constant applied bias with the frequency range of 1 MHz to 0.1 Hz. Open circuit voltage decay (OCVD) was also performed on the same Zahner electrochemical workstation, and the cells were illuminated by a white LED with intensity of 100 mW/cm^2; the transient voltage was recorded

DOI: 10.1021/acs.chemmater.5b03864
Chem. Mater. XXXX, XXX, XXX−XXX

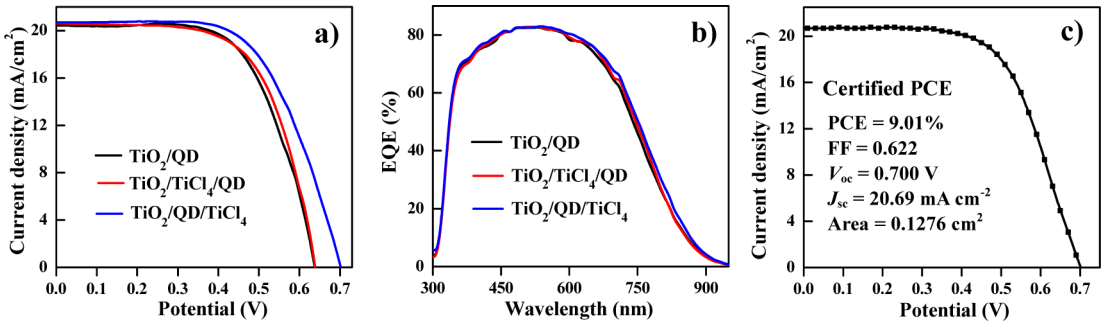

Figure 1. (a and b) $J-V$ curves (a) and EQE (b) of CdSeTe based QDSCs corresponding to photoanodes after different $TiCl_4$ treatment processes. (c) Certified $J-V$ curve of CdSeTe based QDSC with $TiCl_4$ treatment on a sensitized photoanode. Note that the ZnS/SiO_2 layer is omitted in the abbreviation of the samples.

Table 1. Photovoltaic Parameters of Average Values and Standard Deviations for the 5 Devices in Parallel under 1 Full Sun Irradiation for CdSeTe based QDSCs with Different $TiCl_4$ Treatment Processes[a]

Treatment	J_{sc} (mA·cm^{-2})	V_{oc} (V)	FF	PCE (%)
TiO_2/QD	20.60 ± 0.17 (20.70)	0.640 ± 0.004 (0.638)	0.624 ± 0.9 (0.635)	8.23 ± 0.10 (8.39)
TiO_2/$TiCl_4$/QD	20.65 ± 0.12 (20.73)	0.642 ± 0.004 (0.639)	0.626 ± 1.0 (0.637)	8.29 ± 0.09 (8.44)
TiO_2/QD/$TiCl_4$	20.68 ± 0.13 (20.78)	0.702 ± 0.005(0.702)	0.629 ± 1.0 (0.636)	9.13 ± 0.11 (9.28)
TiO_2/QD/$TiCl_4$[b]	20.69	0.700	0.622	9.01

[a]The numbers in parentheses represent the values obtained for the champion cells. [b]Certified cell.

after switching off the light. Transition electron microscopy (TEM) images were obtained using a JEOL JEM-2100 instrument. X-ray diffraction (XRD) patterns were obtained from a Siemens D5005 X-ray powder diffractometer. The absorption spectra of TiO_2 film electrodes (with only 9-μm transparent layer) were recorded on a Shimadzu UV-3101 PC spectrophotometer.

RESULTS AND DISCUSSION

Amorphous TiO_2 Layer Deposition. Two kinds of QDSCs based on CdSe and $CdSe_{0.65}Te_{0.35}$ (simplified as CdSeTe henceforth) QD sensitizers have been prepared. We have chosen CdSe QDs because they are probably the most common QD sensitizer reported, while CdSeTe alloy QDs produced the highest previously reported performance. Results in the main text of the paper focus on the later ones, while the results for the former can be found in the Supporting Information (SI). The 5.2 nm sized CdSeTe QDs with an absorption edge at ~800 nm were chosen as the model QDs, from which the QDSC device with over 8% efficiency has been obtained with a ZnS/SiO_2 barrier layer overcoating.[19,22] The sensitized photoanodes were obtained by the immobilization of a thioglycolic acid (TGA)-capped CdSeTe QD on a TiO_2 mesoporous film electrode through the well-developed capping ligand-induced self-assembly approach,[46,47] which produced a high QD loading, and the corresponding transmission electron microscopy (TEM) images of the CdSeTe QD sensitized TiO_2 film are shown in Figure S1 of the SI. The am-TiO_2 layer was deposited around the sensitized photoanode by immersing the QD sensitized film electrode into a 10.0 mM $TiCl_4$ aqueous solution and storing in an oven at 40 °C for 30 min. The coverage and thickness of the am-TiO_2 layer have been optimized via adjusting $TiCl_4$ solution concentration and soaking temperature and duration. The control experimental results indicate that the performance of the resultant cell devices is insensitive to the treatment temperature (20−70 °C) and time (30−90 min), but dependent on the precursor concentration (0−50 mM), which is similar to the observation of the growth of the metal oxides overlayer in the DSC system.[27] The detailed PCE results of the resulting cell devices dependent on the $TiCl_4$ treatment conditions are available in Table S1. After rinsing with water and ethanol, the am-TiO_2 coated photoanodes were further overcoated sequentially with a ZnS/SiO_2 thin layer according to the literature method.[19] Regenerative sandwich-type cell devices were constructed by combining the obtained photoanode and $Cu_{2-x}S$/FTO counter electrode,[48] followed by filling with S_n^{2-}/S^{2-} electrolyte aqueous solution. For simplicity, the resulting cell is denoted as TiO_2/QD/$TiCl_4$. Note that the ZnS/SiO_2 layer is omitted in the abbreviation of the samples hereafter, but it is important to highlight that this blocking layer is present in all the samples unless something different is specified.

For comparison, reference samples with regular $TiCl_4$ treatment on a plain TiO_2 film electrode followed by sintering at 500 °C for 30 min, a typical procedure used in DSC systems,[30−33] prior to QD sensitization were prepared. These resulting cells are denoted as TiO_2/$TiCl_4$/QD. The cells without $TiCl_4$ treatment on the TiO_2 film electrode were also prepared and denoted as TiO_2/QD. Except for the $TiCl_4$ treatment process, all the other procedures in the construction of the studied cell devices are identical, and the detailed procedures were presented in the Experimental Section. It is noted that, in the case of $TiCl_4$ treatment on a plain TiO_2 electrode, without the subsequent sintering process, the QD loading is low. This leads to relatively low photocurrent and poor PCE of the resultant QDSCs (corresponding absorption spectra and $J-V$ curves are available in Figure S2). The low QD loading in this case may be ascribed to the formation of a loose am-TiO_2 layer around the walls of the mesopore of the film and hindering the penetration of QD particles into the film accordingly (the corresponding structure characterization is discussed below). Therefore, no further discussion is given for this case.

Photovoltaic Performance. The current density−voltage ($J-V$) curves under 1 full sun illumination of the champion cells in each group are shown in Figure 1a, and the photovoltaic parameters of the average values (based on five cells) and

DOI: 10.1021/acs.chemmater.5b03864
Chem. Mater. XXXX, XXX, XXX−XXX

champion cells are listed in Table 1. The detailed $J-V$ curves and photovoltaic parameters for each cell are available in Figure S3 and Table S2. Interestingly, the short-circuit current (J_{sc}, 20.68 vs 20.65 and 20.60 mA/cm^2) and fill factor (FF, 0.629 vs 0.626 and 0.624) remain nearly constant in all these three groups of cells. The observed similar J_{sc} values for all cells that had undergone different $TiCl_4$ treatment processes are in agreement with external quantum yield (EQE) measurement results (Figure 1b), from which similar integrated J_{sc} values for each sample are obtained (20.12, 19.86, and 19.67 mA·cm^{-2} for TiO_2/QD/$TiCl_4$, TiO_2/$TiCl_4$/QD, and TiO_2/QD cells, respectively). However, the V_{oc} of TiO_2/QD/$TiCl_4$ cells is significantly improved to 0.702 V from 0.642 and 0.640 V, corresponding to TiO_2/$TiCl_4$/QD and TiO_2/QD cells, respectively. The average PCE (9.13%) of the TiO_2/QD/$TiCl_4$ cells is superior to those of the reference TiO_2/$TiCl_4$/QD (8.29%) and TiO_2/QD (PCE of 8.23%) cells due to the about 10% photovoltage enhancement. The observed similar photovoltaic performance between TiO_2/$TiCl_4$/QD and TiO_2/QD cells is in accordance with previously reported results.[40,41] It is noted that the small deviation from the average result of five samples as shown in Table 1 indicates the high reproducibility for enhancing the performance of the resulting QDSCs by this facile $TiCl_4$ treatment process. Histograms of photovoltaic performance for a batch of 200 cell samples shown in Figure S4 further highlight the high reproducibility of this approach.

The champion TiO_2/QD/$TiCl_4$ cells exhibit a record PCE of 9.28% (with J_{sc} = 20.78 mA/cm^2; V_{oc} = 0.702 V; FF = 0.636). It is highlighted that the photovoltaic performance of a representative TiO_2/QD/$TiCl_4$ cell was certified by an accredited photovoltaic calibration laboratory (the National Institute of Metrology (NIM) of China) and the certified PCE was 9.01% (Figure 1c, the detailed information for this certification is available in the SI). This result represents a 10% enhancement related to the previous certified record efficiency of 8.2% for QDSCs.[19] Furthermore, our result obtained here pushes the facile QD sensitization technology with a remarkably larger active area (12.76 mm^2) to the same efficiency level of depleted heterojunction solar cells with record efficiency of 8.5% at only 1.37 mm^2 active area.[49,50]

Note that our reported photovoltaic improvement via the am-TiO_2 passivation interface engineering coupled with the ZnS/SiO_2 blocking layer on a sensitized photoanode can also be applied to other QD sensitizers based QDSCs, such as the most commonly studied CdSe based QDSCs. Experimental results indicate that a PCE enhancement of about 10% (7.14% vs 6.50% and 6.43%) can be obtained with the $TiCl_4$ treatment on the sensitized photoanode with the formation of an am-TiO_2 layer between the QD sensitized photoanode and the ZnS/SiO_2 barrier layer in comparison with the $TiCl_4$ treatment on the plain electrode, or no $TiCl_4$ treatment. Detailed photovoltaic parameters for individual cell and average values in each group of CdSe cells together with the $J-V$ curves for the champion cells are available in Table S3 and Figure S5. More interestingly, this 10% enhancement is also ascribed to the ~10% photovoltage enhancement. These results indicate that our developed am-TiO_2 passivation interface engineering with use of $TiCl_4$ treatment on a sensitized photoanode is a generic approach for improving the photovoltage and photovoltaic performance of QDSCs.

Structural Characterization. In order to unveil the intrinsic mechanism of the QDSC performance improvement via the $TiCl_4$ treatment on a sensitized photoanode, structural characterization of the treated electrode was performed with use of high-resolution transition electronic microscopy (HRTEM). As shown in Figure 2a, the lattice planes go straight through the whole TiO_2 particle for TEM imaging of the plain TiO_2 film without $TiCl_4$ treatment, while a ~1.0 nm amorphous layer around the crystalline TiO_2 can be observed from the plain TiO_2 film undergoing a $TiCl_4$ treatment at low temperature (40 °C) but without a subsequent sintering treatment (Figure 2b). This observation indicates that am-TiO_2 is formed in the $TiCl_4$ treatment process due to the hydrolysis and condensation of $TiCl_4$. When the $TiCl_4$ treated plain TiO_2 film undergoes a subsequent high temperature (500 °C) sintering process, the formed am-TiO_2 layer is crystallized and merged into the host substrate (Figure 2c). As for the case of $TiCl_4$ treatment on a sensitized electrode, due to no sintering process in this case, the TEM images (Figure 2d) also show clearly a thin am-TiO_2 layer around the exposed surface of both the TiO_2 particle and QD. To further identify the amorphous or crystalline nature of the formed TiO_2 layer deriving from $TiCl_4$ hydrolysis at 40 °C with or without a subsequent high temperature sintering process, XRD characterization was carried out on the corresponding products. As displayed in the XRD patterns in Figure S6, the obtained product via $TiCl_4$ hydrolysis at 40 °C without a subsequent high temperature sintering process shows no observable diffraction signals, indicating the amorphous nature of the formed product; while for product followed by a sintering process, strong diffraction signals corresponding to crystalline anatase TiO_2 appear. This indicates the initially amorphous product is transferred into crystalline anatase TiO_2 during the sintering process. In order to further confirm the effect of am-TiO_2 layer

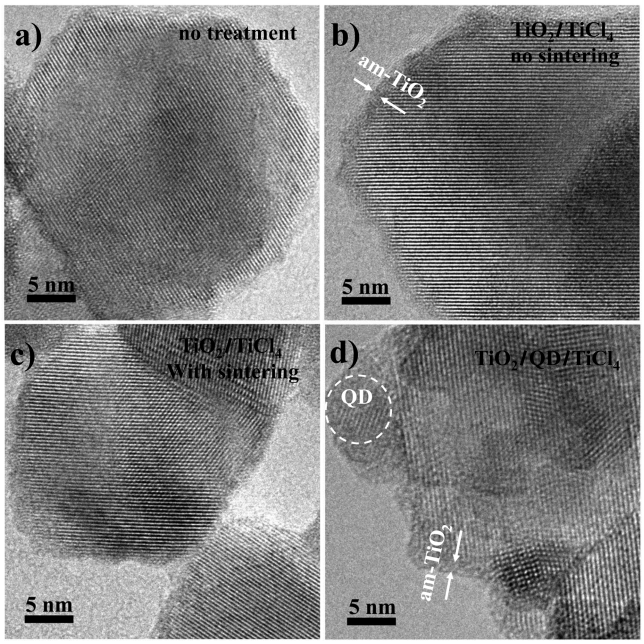

Figure 2. HRTEM images of TiO_2 film electrode after different $TiCl_4$ treatment processes: (a) no treatment, (b) plain film with $TiCl_4$ treatment but no sintering, (c) plain film with $TiCl_4$ treatment followed by sintering process, and (d) QD sensitized film with $TiCl_4$ treatment but no sintering. For clarity, the am-TiO_2 layers are indicated by arrows, and a dashed circle was artificially added around QD.

DOI: 10.1021/acs.chemmater.5b03864
Chem. Mater. XXXX, XXX, XXX−XXX

in suppressing recombination and improving performance, impedance spectroscopy (IS) and photovoltage decay measurements have been carried out.

Impedance Spectroscopy. Impedance Spectroscopy (IS) was widely used in QDSCs to reveal the intrinsic mechanism of photovoltaic performance such as charge transport and recombination, property of counter electrode, and the electrolyte diffusion.[51] Herein, standard fitting models were used to analyze the obtained IS data.[10,52] The detailed complex plane impedance plots measured at different forward biases under dark conditions for all three group of cells are available in Figure S7. The extracted chemical capacitance C_μ, and recombination resistance R_{rec} from the corresponding IS measurements are shown in Figure 3a,b, respectively. The

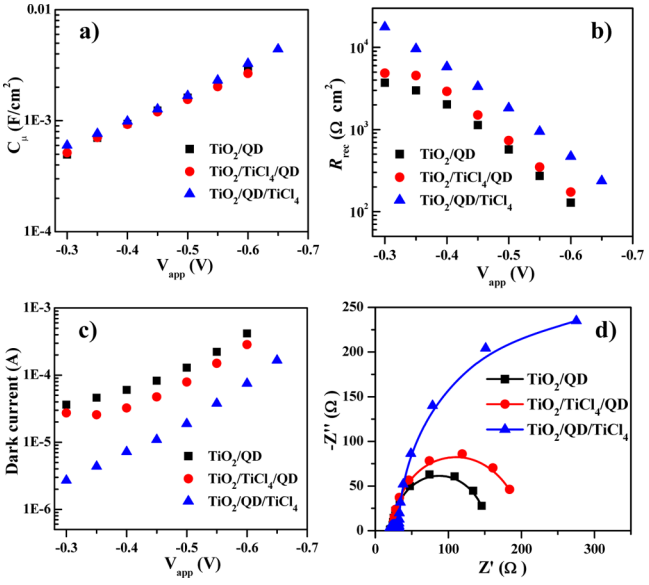

Figure 3. Impedance spectroscopy characterization of the CdSeTe based TiO_2/QD, $TiO_2/TiCl_4$/QD, and TiO_2/QD/$TiCl_4$ cells: (a) chemical capacitance C_μ, (b) recombination resistance R_{rec}, (c) dark current on applied voltage (V_{app}), and (d) Nyquist plots of cells at the forward bias of −0.60 V.

similar C_μ values obtained from the cells with different $TiCl_4$ treatment processes (Figure 3a) reveals that $TiCl_4$ treatment with the formation of am-TiO_2 thin layer does not change the conduction band edge of TiO_2. However, the disparity in the recombination resistance R_{rec} is remarkable for cells with different $TiCl_4$ treatment processes (Figure 3b). It is found that there was no distinct difference in R_{rec} values between the TiO_2/QD and $TiO_2/TiCl_4$/QD cells, whereas the R_{rec} values of TiO_2/QD/$TiCl_4$ cells were several times higher than those of the former two cells under the identical forward bias. Since R_{rec} is inversely proportional to the recombination rate,[51,52] the greater R_{rec} value means the reduced charge recombination rate in TiO_2/QD/$TiCl_4$ cells. Furthermore, the dark current results as shown in Figure 3c also support the conclusion drawn from the R_{rec}. We can find that dark currents of TiO_2/QD/$TiCl_4$ cells were lower than those of TiO_2/QD and $TiO_2/TiCl_4$/QD cells at the same potential. For clarity, direct comparison of Nyquist plots of TiO_2/QD, $TiO_2/TiCl_4$/QD, and TiO_2/QD/$TiCl_4$ cells at a forward bias of −0.60 V is provided in Figure 3d, and the extracted parameters are listed in Table S4. It is found that the R_{rec} value and the calculated electron lifetime ($\tau_n = R_{rec} \times C_\mu$) of the TiO_2/QD/$TiCl_4$ cell are more than three times higher than those of TiO_2/QD and $TiO_2/TiCl_4$/QD cells. Overall, the IS results show that the am-TiO_2 thin layer coated around the sensitized photoanode plays a dramatic role in inhibiting electron recombination at the TiO_2/QD/electrolyte interfaces, enhancing even higher the significant effect already reported for the ZnS/SiO_2 blocking layer.

Open-Circuit Voltage-Decay Measurement. In addition to IS, the reduced charge recombination kinetics in TiO_2/QD/$TiCl_4$ cells relative to $TiO_2/TiCl_4$/QD and TiO_2/QD cells was independently analyzed using an alternative characterization by open-circuit voltage-decay (OCVD) measurement. Figure 4a

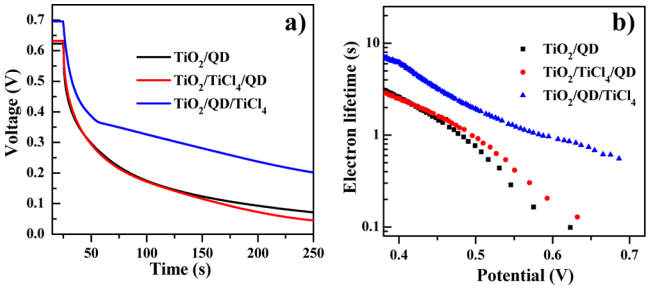

Figure 4. (a) Open circuit decay curves of CdSeTe based TiO_2/QD, $TiO_2/TiCl_4$/QD, and TiO_2/QD/$TiCl_4$ cells; (b) calculated electron lifetime derived from the V_{oc} decay measurements.

depicts the continued monitoring of V_{oc}, starting from steady state under illumination followed by the V_{oc} decay after switching off the illumination.[53−56] The voltage decay rate for the TiO_2/QD/$TiCl_4$ cell was remarkably slower than the other two cells, which are almost at the same level. The voltage decay rate can provide information about the recombination of the photogenerated electrons with oxidized species in the electrolyte, and the electron lifetime (τ_n) can be calculated according to the equation $\tau_n = -(k_BT/e)(dV_{oc}/dt)^{-1}$, where k_B is the Boltzmann constant, T is the absolute temperature (298 K), and e is the electronic charge.[57] As shown in Figure 4b, the electron lifetime of all the cells increases with decreasing V_{oc} due to the reduction of trapped carrier density, and the electron lifetime of TiO_2/QD/$TiCl_4$ cell was 3−4 times longer than the others for the same voltage condition. Since the densities of states of both films are similar, as indicated by the chemical capacitance results, the longer lifetime of the TiO_2/QD/$TiCl_4$ cell confirms the suppressed recombination of photogenerated electrons. This result is in good agreement and confirms the IS studies pointing to a reduction of recombination when am-TiO_2 is used between the QD sensitized electrode and the ZnS/SiO_2 blocking layer.

Interface Passivation/Buffering Effect for am-TiO_2 Layer. The above-mentioned results demonstrate the importance of the am-TiO_2 layer in improving the photovoltaic performance of QDSCs with the presence of a ZnS/SiO_2 barrier layer. Meanwhile, previous theoretical results revealed that the wide band gap and insulator ZnS/SiO_2 coating on a TiO_2 substrate reduced the density of surface states (DOS) by 3 orders of magnitude.[19] This fact indicates that the adopted ZnS/SiO_2 barrier layer should be strong enough to block the photogenerated electron leakage from photoanode to electrolyte. The question of what is the exact role that am-TiO_2 layer takes in improving the performance of QDSC comes out naturally. To elucidate the mechanism of the am-TiO_2 layer in enhancing the performance of QDSCs, a series of controlled experiments were carried out.

DOI: 10.1021/acs.chemmater.5b03864
Chem. Mater. XXXX, XXX, XXX−XXX

Table 2. Average Photovoltaic Parameters of 5 Cells in Parallel under 1 Full Sun Irradiation for CdSeTe Based QDSCs with Different Overcoating Layers around a Sensitized Photoanode

Cells	J_{sc} (mA·cm^{-2})	V_{oc} (V)	FF	PCE (%)
TiO_2/QD/am-TiO_2	12.35	0.576	0.644	4.58 ± 0.08
TiO_2/QD/am-TiO_2/ZnS	20.16	0.636	0.619	7.94 ± 0.10
TiO_2/QD/am-TiO_2/SiO_2	14.17	0.641	0.621	5.65 ± 0.09
TiO_2/QD/ZnS/SiO_2	20.60	0.640	0.624	8.23 ± 0.10
TiO_2/QD/am-TiO_2/ZnS/SiO_2	20.68	0.702	0.629	9.13 ± 0.11
TiO_2/QD/ZnS/am-TiO_2/SiO_2	17.63	0.647	0.648	7.39 ± 0.12
TiO_2/QD/ZnS/SiO_2/am-TiO_2	15.99	0.646	0.661	6.83 ± 0.09

First, the photovoltaic performance of the CdSeTe solar cells corresponding to the sole am-TiO_2 layer (noted as TiO_2/QD/am-TiO_2) was measured. Meanwhile, to highlight the effect of the ZnS/SiO_2 double layer, the performances of cells with a single ZnS or SiO_2 layer (TiO_2/QD/am-TiO_2/ZnS, TiO_2/QD/am-TiO_2/SiO_2) were also instigated and the results are shown in Table 2. From these results we can find that, in serving as an energy barrier layer to reduce recombination and enhance the performance, the effect of am-TiO_2 or the recombination of am-TiO_2 with single ZnS or SiO_2 is remarkably weaker than that of ZnS/SiO_2, and of am-TiO_2/ZnS/SiO_2. To further confirm the buffer layer effect of the am-TiO_2 layer, the am-TiO_2 layer was intentionally placed into different interfaces in the TiO_2/QD/ZnS/SiO_2 photoanode system, and the photovoltaic performance from the corresponding cell devices was evaluated and listed in Table 2. When the am-TiO_2 layer was placed between ZnS and SiO_2 coating layers (i.e., TiO_2/QD/ZnS/am-TiO_2/SiO_2) or outside the ZnS/SiO_2 layer (i.e., TiO_2/QD/ZnS/SiO_2/am-TiO_2), the PCE/J_{sc} of resultant cells decreased to 7.39%/17.53 mA cm^{-2} and 6.83%/15.99 mA cm^{-2}, respectively, while the V_{oc} remained at the same level as that of the regular TiO_2/QD/ZnS/SiO_2 based cells. These data indicate clearly that the am-TiO_2 layer can have a favorable effect on enhancing the photovoltages of the cell devices only when the am-TiO_2 layer is located on the interface between the QD sensitized photoanode and the ZnS/SiO_2 barrier layer. Otherwise, it will have detrimental effects.

The most significant effect of the ZnS/SiO_2 blocking layer (without am-TiO_2) is the reduction of the recombination of photoinjected electrons into the TiO_2 with the accepting species in the sensitizer/electrolyte.[19] This recombination is especially significant in QDSCs in comparison with DSCs, as there is a large portion of TiO_2 surface uncovered. Concerning the role of am-TiO_2 and based on the data here reported, there are two important aspects of the TiO_2 coating in order to attain a significant enhancement of the final PCE. First, the layer has to be amorphous. am-TiO_2 is superior to crystalline TiO_2 in acting as the passivation/buffer layer between the QD sensitized photoanode and the ZnS/SiO_2 interface. In our experiments, with results shown in Table S5, we find that, in the case of no am-TiO_2 layer (i.e., no $TiCl_4$ aqueous solution treatment on the photoanode), the PCEs of CdSe based QDSCs can be enhanced from 6.41% to 6.57% when the sensitized photoanode (i.e., TiO_2/QD/ZnS/SiO_2) is subjected to a sintering treatment at 300 °C for 2 min in air atmosphere. This finding is in accordance with previous reports.[47,58,59] While, in the case of the presence of an am-TiO_2 layer (i.e., $TiCl_4$ treatment on a CdSe QD sensitized photoanode performed, TiO_2/QD/am-TiO_2/ZnS/SiO_2), the identical sintering treatment of the photoanode cannot cause an increase, but a reduction of PCE of the resultant QDSCs from 7.11 to 6.45%. Undoubtedly, this PCE reduction should be ascribed to the transfer of initially formed am-TiO_2 into crystalline TiO_2 during the high-temperature sintering process. This finding clearly demonstrates the advantage of am-TiO_2 in comparison with crystalline TiO_2 in serving as the passivation/buffer layer between the QD sensitized photoanode and the ZnS/SiO_2 interface.

Second, the am-TiO_2 has to be in contact with the uncovered mesoporous TiO_2 surface. A plausible mechanism for am-TiO_2 in the performance improvement should be that the am-TiO_2 layer acts as a passivation/buffer layer at the interface between the QD sensitized photoanode and ZnS/SiO_2 barrier layer. Amorphous layer passivates the crystalline mesoporous TiO_2 surface, as recrystallization of this layer just change the size of the particles but not the basic nature of the surface including surface states. In addition, am-TiO_2 also provides an excellent buffer for the ZnS/SiO_2 blocking layer. Consequently, charge recombination is reduced, and the performance of cells is improved. Lattice mismatch between the TiO_2 and ZnS (7%) as well as CdSeTe and SiO_2 (14%),[24] is fairly accommodated by the amorphous buffer. The use of extra passivation/buffer layer has been extensively performed in developing highly luminescent core/shell structured QD systems.[60]

CONCLUSIONS

In summary, controlling the surface properties to modify the complicated interface plays a critical role in designing high efficiency QDSCs. Herein, we provide an interface engineering modification method for QDSCs using am-TiO_2 via a facile hydrolysis of $TiCl_4$ on QD sensitized photoanodes before the ZnS/SiO_2 coating. It is demonstrated that the presence of an am-TiO_2 layer at the interface between the surface of a mesoporous TiO_2 substrate and a QD light-absorber and the ZnS/SiO_2 blocking layer is capable of reducing substantially the device recombination and therefore boosting PCEs beyond 9%. The PCE enhancement is due to the improvement of V_{oc} while J_{sc} and FF remain unchanged after the addition of an am-TiO_2 coating. Results reported here imply a significant 10% increase of the certified record efficiencies for QDSCs. The am-TiO_2 layer shows greater advantage in serving as passivation/buffer layer for suppressing interface recombination and improving the performance of QDSCs in comparison with crystalline TiO_2. Due to the facility and generality of this treatment in drastically improving the performance of QDSCs, this technique could be used in exploiting the potential of QDSCs and in opening up new opportunities to further improve the performance of QDSCs up to an efficiency level of more than 10%: the threshold for commercial application. Control of recombination and further optimization of electrolyte and counter electrode will contribute to further increasing the reported efficiencies for QDSCs in the near future.

DOI: 10.1021/acs.chemmater.5b03864
Chem. Mater. XXXX, XXX, XXX−XXX

■ ASSOCIATED CONTENT

Supporting Information

The Supporting Information is available free of charge on the ACS Publications website at DOI: 10.1021/acs.chemmater.5b03864.

TEM characterization of plain and CdSeTe sensitized films. $J-V$ curves and photovoltaic parameters of CdSeTe and CdSe based cell devices (each group has 5 devices in parallel) that had undergone different $TiCl_4$ treatments. Certified report for photovoltaic performance of CdSeTe cell. XRD measurement of FTO substrate with the $TiCl_4$ treatment after sintering or no sintering. Nyquist curves under different bias voltages and impedance values at −0.6 V forward bias for CdSeTe based cells. (PDF)

■ AUTHOR INFORMATION

Corresponding Author

*E-mail: zhongxh@ecust.edu.cn. Tel/Fax: (+86) 21 6425 0281.

Author Contributions

⊥Z.R. and J.W. contributed equally.

Notes

The authors declare no competing financial interest.

■ ACKNOWLEDGMENTS

This research is supported by the National Natural Science Foundation of China (nos. 91433106, 21421004), the Fundamental Research Funds for the Central Universities in China, and the Generalitat Valenciana Project (PROMETEO/2014/020).

■ REFERENCES

(1) Swierk, J. R.; Mallouk, T. E. Design and Development of Photoanodes for Water-Splitting Dye-Sensitized Photoelectrochemical Cells. *Chem. Soc. Rev.* **2013**, *42*, 2357−2387.

(2) Hagfeldt, A.; Boschloo, G.; Sun, L. C.; Kloo, L.; Pettersson, H. Dye-Sensitized Solar Cells. *Chem. Rev.* **2010**, *110*, 6595−6663.

(3) Roelofs, K. E.; Brennan, T. P.; Bent, S. F. Interface Engineering in Inorganic-Absorber Nanostructured Solar Cells. *J. Phys. Chem. Lett.* **2014**, *5*, 348−360.

(4) Kershaw, S. V.; Susha, A. S.; Rogach, A. L. Narrow Bandgap Colloidal Metal Chalcogenide Quantum Dots: Synthetic Methods, Heterostructures, Assemblies, Electronic and Infrared Optical Properties. *Chem. Soc. Rev.* **2013**, *42*, 3033−3087.

(5) Lohse, S. E.; Murphy, C. J. Applications of Colloidal Inorganic Nanoparticles: From Medicine to Energy. *J. Am. Chem. Soc.* **2012**, *134*, 15607−15620.

(6) Kramer, I. J.; Sargent, E. H. The Architecture of Colloidal Quantum Dot Solar Cells: Materials to Devices. *Chem. Rev.* **2014**, *114*, 863−882.

(7) Nozik, A. J.; Beard, M. C.; Luther, J. M.; Law, M.; Ellingson, R. J.; Johnson, J. C. Semiconductor Quantum Dots and Quantum Dot Arrays and Applications of Multiple Exciton Generation to Third-Generation Photovoltaic Solar Cells. *Chem. Rev.* **2010**, *110*, 6873−6890.

(8) Palmstrom, A. F.; Santra, P. K.; Bent, S. F. Atomic Layer Deposition in Nanostructured Photovoltaics: Tuning Optical, Electronic and Surface Properties. *Nanoscale* **2015**, *7*, 12266−12283.

(9) Kamat, P. V. Boosting the Efficiency of Quantum Dot Sensitized Solar Cells through Modulation of Interfacial Charge Transfer. *Acc. Chem. Res.* **2012**, *45*, 1906−1915.

(10) Mora-Seró, I.; Gimenez, S.; Fabregat-Santiago, F.; Gomez, R.; Shen, Q.; Toyoda, T.; Bisquert, J. Recombination in Quantum Dot Sensitized Solar Cells. *Acc. Chem. Res.* **2009**, *42*, 1848−1857.

(11) Hodes, G. Comparison of Dye- and Semiconductor-Sensitized Porous Nanocrystalline Liquid Junction Solar Cells. *J. Phys. Chem. C* **2008**, *112*, 17778−17787.

(12) Pan, Z. X.; Mora-Seró, I.; Shen, Q.; Zhang, H.; Li, Y.; Zhao, K.; Wang, J.; Zhong, X. H.; Bisquert, J. High-Efficiency "Green" Quantum Dot Solar Cells. *J. Am. Chem. Soc.* **2014**, *136*, 9203−9210.

(13) Lan, X. Z.; Masala, S.; Sargent, E. H. Charge-Extraction Strategies for Colloidal Quantum Dot Photovoltaics. *Nat. Mater.* **2014**, *13*, 233−240.

(14) Grätzel, M.; Janssen, R. A.; Mitzi, D. B.; Sargent, E. H. Materials Interface Engineering for Solution-Processed Photovoltaics. *Nature* **2012**, *488*, 304−312.

(15) Sahasrabudhe, A.; Bhattacharyya, S. Dual Sensitization Strategy for High-Performance Core/Shell/Quasi-shell Quantum Dot Solar Cells. *Chem. Mater.* **2015**, *27*, 4848−4859.

(16) Yan, K. Y.; Zhang, L. X.; Qiu, J. H.; Qiu, Y. C.; Zhu, Z. L.; Wang, J. N.; Yang, S. H. A Quasi-Quantum Well Sensitized Solar Cell with Accelerated Charge Separation and Collection. *J. Am. Chem. Soc.* **2013**, *135*, 9531−9539.

(17) Wei, H. Y.; Wang, G. S.; Luo, Y. H.; Li, D. M.; Meng, Q. B. Investigation on Interfacial Charge Transfer Process in $CdSe_xTe_{1-x}$ Alloyed Quantum Dot Sensitized Solar Cells. *Electrochim. Acta* **2015**, *173*, 156−163.

(18) Tian, J. J.; Lv, L. L.; Fei, C. B.; Wang, Y. J.; Liu, X. G.; Cao, G. Z. A Highly Efficient (>6%) $Cd_{1-x}Mn_xSe$ Quantum Dot Sensitized Solar Cell. *J. Mater. Chem. A* **2014**, *2*, 19653−19659.

(19) Zhao, K.; Pan, Z. X.; Mora-Seró, I.; Cánovas, E.; Wang, H.; Song, Y.; Gong, X. Q.; Wang, J.; Bonn, M.; Bisquert, J.; Zhong, X. H. Boosting Power Conversion Efficiencies of Quantum-Dot-Sensitized Solar Cells Beyond 8% by Recombination Control. *J. Am. Chem. Soc.* **2015**, *137*, 5602−5609.

(20) Jiao, S.; Shen, Q.; Mora-Seró, I.; Wang, J.; Pan, Z. X.; Zhao, K.; Kuga, Y.; Zhong, X. H.; Bisquert, J. Band Engineering in Core/Shell ZnTe/CdSe for Photovoltage and Efficiency Enhancement in Exciplex Quantum Dot Sensitized Solar Cells. *ACS Nano* **2015**, *9*, 908−915.

(21) Wang, J.; Mora-Seró, I.; Pan, Z. X.; Zhao, K.; Zhang, H.; Feng, Y. Y.; Yang, G.; Zhong, X. H.; Bisquert, J. Core/Shell Colloidal Quantum Dot Exciplex States for the Development of Highly Efficient Quantum-Dot-Sensitized Solar Cells. *J. Am. Chem. Soc.* **2013**, *135*, 15913−15922.

(22) Pan, Z. X.; Zhao, K.; Wang, J.; Zhang, H.; Feng, Y. Y.; Zhong, X. H. Near Infrared Absorption of $CdSe_xTe_{1-x}$ Alloyed Quantum Dot Sensitized Solar Cells with More than 6% Efficiency and High Stability. *ACS Nano* **2013**, *7*, 5215−5222.

(23) Lee, M. M.; Teuscher, J.; Miyasaka, T.; Murakami, T. N.; Snaith, H. J. Efficient Hybrid Solar Cells Based on Meso-Superstructured Organometal Halide Perovskites. *Science* **2012**, *338*, 643−647.

(24) Dabbousi, B. O.; Rodriguez-Viejo, J.; Mikulec, F. V.; Heine, J. R.; Mattoussi, H.; Ober, R.; Jensen, K. F.; Bawendi, M. G. CdSe)ZnS Core−Shell Quantum Dots: Synthesis and Characterization of a Size Series of Highly Luminescent Nanocrystallites. *J. Phys. Chem. B* **1997**, *101*, 9463−9475.

(25) Mu, L. L.; Liu, C. M.; Jia, J. G.; Zhou, X. W.; Lin, Y. Dual Post-Treatment: A Strategy Towards High Efficiency Quantum Dot Sensitized Solar Cells. *J. Mater. Chem. A* **2013**, *1*, 8353−8357.

(26) Kay, A.; Grätzel, M. Dye-Sensitized Core−Shell Nanocrystals: Improved Efficiency of Mesoporous Tin Oxide Electrodes Coated with a Thin Layer of an Insulating Oxide. *Chem. Mater.* **2002**, *14*, 2930−2935.

(27) Palomares, E.; Clifford, J. N.; Haque, S. A.; Lutz, T.; Durrant, J. R. Control of Charge Recombination Dynamics in Dye Sensitized Solar Cells by the Use of Conformally Deposited Metal Oxide Blocking Layers. *J. Am. Chem. Soc.* **2003**, *125*, 475−482.

(28) Son, H.-J.; Wang, X. W.; Prasittichai, C.; Jeong, N. C.; Aaltonen, T.; Gordon, R. G.; Hupp, J. T. Glass-Encapsulated Light Harvesters: More Efficient Dye-Sensitized Solar Cells by Deposition of Self-Aligned, Conformal, and Self-Limited Silica Layers. *J. Am. Chem. Soc.* **2012**, *134*, 9537−9540.

DOI: 10.1021/acs.chemmater.5b03864
Chem. Mater. XXXX, XXX, XXX−XXX

(29) Chandiran, A. K.; Nazeeruddin, M. K.; Grätzel, M. The Role of Insulating Oxides in Blocking the Charge Carrier Recombination in Dye-Sensitized Solar Cells. *Adv. Funct. Mater.* **2014**, *24*, 1615−1623.
(30) Nazeeruddin, M. K.; Kay, A.; Rodicio, I.; Humphry-Baker, R.; Müller, E.; Liska, P.; Vlachopoulos, N.; Grätzel, M. Conversion of Light to Electricity by *cis*-X_2Bis(2,2′-bipyridyl-4,4′-dicarboxylate)-ruthenium(II) Charge-Transfer Sensitizers (X = Cl-, Br-, I-, CN-, and SCN-) on Nanocrystalline Titanium Dioxide Electrodes. *J. Am. Chem. Soc.* **1993**, *115*, 6382−6390.
(31) Sommeling, P. M.; O'Regan, B. C.; Haswell, R. R.; Smit, H. J. P.; Bakker, N. J.; Smits, J. J. T.; Kroon, J. M.; van Roosmalen, J. A. M. Influence of a $TiCl_4$ Post-Treatment on Nanocrystalline TiO_2 Films in Dye-Sensitized Solar Cells. *J. Phys. Chem. B* **2006**, *110*, 19191−19197.
(32) Lee, S.-W.; Ahn, K.-S.; Zhu, K.; Neale, N. R.; Frank, A. J. Effects of $TiCl_4$ Treatment of Nanoporous TiO_2 Films on Morphology, Light Harvesting, and Charge-Carrier Dynamics in Dye-Sensitized Solar Cells. *J. Phys. Chem. C* **2012**, *116*, 21285−21290.
(33) Fuke, N.; Katoh, R.; Islam, A.; Kasuya, M.; Furube, A.; Fukui, A.; Chiba, Y.; Komiya, R.; Yamanaka, R.; Han, L. Y.; Harima, H. Influence of $TiCl_4$ Treatment on Back Contact Dye-Sensitized Solar Cells Sensitized with Black Dye. *Energy Environ. Sci.* **2009**, *2*, 1205−1209.
(34) Diguna, L. J.; Shen, Q.; Kobayashi, J.; Toyoda, T. High Efficiency of CdSe Quantum-Dot-Sensitized TiO_2 Inverse Opal Solar Cells. *Appl. Phys. Lett.* **2007**, *91*, 023116.
(35) Shalom, M.; Dor, S.; Ruhle, S.; Grinis, L.; Zaban, A. Core/CdS Quantum Dot/Shell Mesoporous Solar Cells with Improved Stability and Efficiency Using an Amorphous TiO_2 Coating. *J. Phys. Chem. C* **2009**, *113*, 3895−3898.
(36) Liu, Z. F.; Miyauchi, M.; Uemura, Y.; Cui, Y.; Hara, K.; Zhao, Z. G.; Sunahara, K.; Furube, A. Enhancing the Performance of Quantum Dots Sensitized Solar Cell by SiO_2 Surface Coating. *Appl. Phys. Lett.* **2010**, *96*, 233107.
(37) Roelofs, K. E.; Brennan, T. P.; Dominguez, J. C.; Bailie, C. D.; Margulis, G. Y.; Hoke, E. T.; McGehee, M. D.; Bent, S. F. Effect of Al_2O_3 Recombination Barrier Layers Deposited by Atomic Layer Deposition in Solid-State CdS Quantum Dot-Sensitized Solar Cells. *J. Phys. Chem. C* **2013**, *117*, 5584−5592.
(38) Tachan, Z.; Hod, I.; Shalom, M.; Grinis, L.; Zaban, A. The Importance of the TiO_2/Quantum Dots Interface in the Recombination Processes of Quantum Dot Sensitized Solar Cells. *Phys. Chem. Chem. Phys.* **2013**, *15*, 3841−3845.
(39) Barea, E.; Xu, X. Q.; González-Pedro, V.; Ripollés-Sanchis, T.; Fabregat-Santiago, F.; Bisquert, J. Origin of Efficiency Enhancement in Nb_2O_5 Coated Titanium Dioxide Nanorod Based Dye Sensitized Solar Cells. *Energy Environ. Sci.* **2011**, *4*, 3414−3419.
(40) Samadpour, M.; Boix, P.; Gimenez, S.; Iraji Zad, A.; Taghavinia, N.; Mora-Seró, I.; Bisquert, J. Fluorine Treatment of TiO_2 for Enhancing Quantum Dot Sensitized Solar Cell Performance. *J. Phys. Chem. C* **2011**, *115*, 14400−14407.
(41) Du, Z. L.; Zhang, H.; Bao, H. L.; Zhong, X. H. Optimization of TiO_2 Photoanode Films for Highly Efficient Quantum Dot-Sensitized Solar Cells. *J. Mater. Chem. A* **2014**, *2*, 13033−13040.
(42) Kim, J.; Choi, H.; Nahm, C.; Kim, C.; Nam, S.; Kang, S.; Jung, D.-R.; Kim, J. I.; Kang, J.; Park, B. The Role of a $TiCl_4$ Treatment on the Performance of CdS Quantum-Dot-Sensitized Solar Cells. *J. Power Sources* **2012**, *220*, 108−113.
(43) Hwang, J.-Y.; Lee, S.-A.; Lee, Y. H.; Seok, S.-I. Improved Photovoltaic Response of Nanocrystalline CdS-Sensitized Solar Cells through Interface Control. *ACS Appl. Mater. Interfaces* **2010**, *2*, 1343−1348.
(44) Shalom, M.; Albero, J.; Tachan, Z.; Martínez-Ferrero, E.; Zaban, A.; Palomares, E. Quantum Dot-Dye Bilayer-Sensitized Solar Cells: Breaking the Limits Imposed by the Low Absorbance of Dye Monolayers. *J. Phys. Chem. Lett.* **2010**, *1*, 1134−1138.
(45) Xie, Z.; Liu, X. X.; Wang, W. P.; Wang, X. J.; Liu, C.; Xie, Q.; Li, Z. C.; Zhang, Z. J. Enhanced Photoelectrochemical and Photocatalytic Performance of TiO_2 Nanorod Arrays/CdS Quantum Dots by Coating TiO_2 through Atomic Layer Deposition. *Nano Energy* **2015**, *11*, 400−408.
(46) Zhang, H.; Cheng, K.; Hou, Y. M.; Fang, Z.; Pan, Z. X.; Wu, W. J.; Hua, J. L.; Zhong, X. H. Efficient CdSe Quantum Dot-Sensitized Solar Cells Prepared by Postsynthesis Assembly Approach. *Chem. Commun.* **2012**, *48*, 11235−11237.
(47) Li, W. J.; Zhong, X. H. Capping Ligand-Induced Self-Assembly for Quantum Dot Sensitized Solar Cells. *J. Phys. Chem. Lett.* **2015**, *6*, 796−806.
(48) Zhang, H.; Bao, H. L.; Zhong, X. H. Highly Efficient, Stable and Reproducible CdSe-Sensitized Solar Cells Using Copper Sulfide as Counter Electrodes. *J. Mater. Chem. A* **2015**, *3*, 6557−6564.
(49) Chuang, C. H. M.; Brown, P. R.; Bulovic, V.; Bawendi, M. G. Improved Performance and Stability in Quantum Dot Solar Cells through Band Alignment Engineering. *Nat. Mater.* **2014**, *13*, 796−801.
(50) Ning, Z. J.; Voznyy, O.; Pan, J.; Hoogland, S.; Adinolfi, V.; Xu, J. X.; Li, M.; Kirmani, A. R.; Sun, J.-P.; Minor, J.; Kemp, K. W.; Dong, H.; Rollny, L.; Labelle, A.; Carey, G.; Sutherland, B.; Hill, I.; Amassian, A.; Liu, H.; Tang, J.; Bakr, O. M.; Sargent, E. H. Air-Stable n-Type Colloidal Quantum Dot Solids. *Nat. Mater.* **2014**, *13*, 822−828.
(51) Fabregat-Santiago, F.; Garcia-Belmonte, G.; Mora-Seró, I.; Bisquert, J. Characterization of Nanostructured Hybrid and Organic Solar Cells by Impedance Spectroscopy. *Phys. Chem. Chem. Phys.* **2011**, *13*, 9083−9118.
(52) González-Pedro, V.; Xu, X. Q.; Mora-Seró, I.; Bisquert, J. Modeling High-Efficiency Quantum Dot Sensitized Solar Cells. *ACS Nano* **2010**, *4*, 5783−5790.
(53) Zaban, A.; Greenshtein, M.; Bisquert, J. Determination of the Electron Lifetime in Nanocrystalline Dye Solar Cells by Open-Circuit Voltage Decay Measurements. *ChemPhysChem* **2003**, *4*, 859−864.
(54) Xu, C. K.; Shin, P. H.; Cao, L. L.; Wu, J. M.; Gao, D. Ordered TiO_2 Nanotube Arrays on Transparent Conductive Oxide for Dye-Sensitized Solar Cells. *Chem. Mater.* **2010**, *22*, 143−148.
(55) Wu, W. Q.; Liao, J. Y.; Chen, H. Y.; Yu, X. Y.; Su, C. Y.; Kuang, D. B. Dye-Sensitized Solar Cells Based on a Double Layered TiO_2 Photoanode Consisting of Hierarchical Nanowire Arrays and Nanoparticles with Greatly Improved Photovoltaic Performance. *J. Mater. Chem.* **2012**, *22*, 18057−18062.
(56) Zhang, M.; Zhang, J.; Fan, Y.; Yang, L.; Wang, Y. L.; Li, R. Z.; Wang, P. Judicious Selection of a Pinhole Defect Filler to Generally Enhance the Performance of Organic Dye-Sensitized Solar Cells. *Energy Environ. Sci.* **2013**, *6*, 2939−2943.
(57) Bisquert, J.; Zaban, A.; Greenshtein, M.; Mora-Seró, I. Determination of Rate Constants for Charge Transfer and the Distribution of Semiconductor and Electrolyte Electronic Energy Levels in Dye-Sensitized Solar Cells by Open-Circuit Photovoltage Decay Method. *J. Am. Chem. Soc.* **2004**, *126*, 13550−13559.
(58) Fan, S.-Q.; Fang, B.; Kim, J. H.; Kim, J.-J.; Yu, J.-S.; Ko, J. Hierarchical Nanostructured Spherical Carbon with Hollow Core/Mesoporous Shell as a Highly Efficient Counter Electrode in CdSe Quantum-Dot-Sensitized Solar Cells. *Appl. Phys. Lett.* **2010**, *96*, 063501.
(59) Pan, Z. X.; Zhang, H.; Cheng, K.; Hou, Y. M.; Hua, J. L.; Zhong, X. H. Highly Efficient Inverted Type-I CdS/CdSe Core/Shell Structure QD-Sensitized Solar Cells. *ACS Nano* **2012**, *6*, 3982−3991.
(60) Xie, R. G.; Kolb, U.; Li, J. X.; Basché, T.; Mews, A. Synthesis and Characterization of Highly Luminescent CdSe−Core CdS/$Zn_{0.5}Cd_{0.5}S$/ZnS Multishell Nanocrystals. *J. Am. Chem. Soc.* **2005**, *127*, 7480−7488.

DOI: 10.1021/acs.chemmater.5b03864
Chem. Mater. XXXX, XXX, XXX−XXX